Comparative study of exchange-correlation functionals for accurate predictions of structural and magnetic properties of multiferroic oxides

Hanghui Chen and Andrew J. Millis

A comparative study of exchange-correlation functionals for accurate predictions of structural and magnetic properties of multiferroic oxides

Hanghui Chen[1,2] and Andrew J. Millis[1]

[1]*Department of Physics,*

Columbia University,

New York, NY, 10027, USA

[2]*Department of Applied Physics and Applied Mathematics,*

Columbia University,

New York, NY, 10027, USA

Abstract

We systematically compare predictions of various exchange correlation functionals for the structural and magnetic properties of perovskite $Sr_{1-x}Ba_xMnO_3$ ($0 \leq x \leq 1$) – a representative class of multiferroic oxides. The local spin density approximation (LSDA) and spin-dependent generalized gradient approximation with Perdew-Burke-Ernzerhof parameterization (sPBE) make substantial different predictions for ferroelectric atomic distortions, tetragonality and ground state magnetic ordering. Neither approximation quantitatively reproduces all the measured structural and magnetic properties of perovskite $Sr_{0.5}Ba_{0.5}MnO_3$. The spin-dependent generalized gradient approximation with Perdew-Burke-Ernzerhof revised for solids parameterization (sPBEsol) and the charge-only Perdew-Burke-Ernzerhof parameterized generalized gradient approximation with Hubbard U and Hund's J extensions both provide overall better agreement with measured structural and magnetic properties of $Sr_{0.5}Ba_{0.5}MnO_3$, compared to LSDA and sPBE. Using these two methods, we find that different from previous predictions, perovskite $BaMnO_3$ has large Mn off-center displacements and is close to a ferromagnetic-to-antiferromagnetic phase boundary, making it a promising candidate to induce effective giant magnetoelectric effects and to achieve cross-field control of polarization and magnetism.

I. INTRODUCTION

Searching for multiferroic materials, in particular those simultaneously possessing ferroelectric polarization and ferromagnetic moments with strong coupling between the two order parameters, is currently of great interest due to their potential applications in multifunctional electronics where low-voltage control of magnetism is desirable [1, 2]. *Ab initio* density functional theory (DFT) based calculations are an important tool for identifying appropriate candidate materials. However, different density functionals can produce quantitatively different predictions for physical properties. For example, the widely used local density approximation (LDA) underestimates unit cell volumes, while the generalized gradient approximation with Perdew-Burke-Ernzerhof parameterization (PBE) overestimates unit cell volumes. While the uncertainty is acceptable in many contexts, ferroelectric instabilities are sensitive to volume changes and may be incorrectly predicted. In particular, PBE predicts an incorrect supertetragonal structure in $BaTiO_3$ and $PbTiO_3$ [3, 4]. Recent studies [5–7] also show that magnetic properties may not be correctly predicted by local spin density approximation (LSDA) and spin-dependent generalized gradient approximation with Perdew-Burke-Ernzerhof parameterization (sPBE) because these approximations imply an intrinsic effective exchange coupling which is unphysically large for transition metal d-orbitals. These issues motivate a careful examination of the predictions from different exchange correlation functionals in the multiferroic context.

In this paper, we investigate predictions of different density functionals for the structural and magnetic properties of a representative class of magnetic ferroelectrics $Sr_{1-x}Ba_xMnO_3$. Specific members of this family were previously investigated with specific density functionals. For example, Rondinelli *et. al.* used LSDA to investigate perovskite $BaMnO_3$ [8]; Giovannetti *et. al.* used sPBE [9] while Nourafkan *et. al.* employed LSDA [10] to study perovskite $Sr_{0.5}Ba_{0.5}MnO_3$. Sondena [11] *et. al.* used sPBE to investigate cubic perovskite $SrMnO_3$ while Lee [12] *et. al.* used both sPBE and LSDA to investigate perovskite $SrMnO_3$ under epitaxial strain. The new features of our work are that we document the substantial differences between LSDA and sPBE in the predictions for the ferroelectric polar distortions, c/a ratio (c is the out-of-plane lattice constant and a is the in-plane lattice constant) and ground state magnetic ordering of perovskite $Sr_{1-x}Ba_xMnO_3$ (Ref. [12] also noted the differences between LSDA and sPBE for properties of strained $SrMnO_3$). Comparing to the available

experimental data for $Sr_{0.5}Ba_{0.5}MnO_3$ [13], we find that neither LSDA nor sPBE can, at the same time, accurately predict both structural and magnetic properties. However, we show that two alternative exchange correlation functionals provide a more accurate description of the properties of $Sr_{0.5}Ba_{0.5}MnO_3$. One is the spin-dependent generalized gradient approximation with Perdew-Burke-Ernzerhof revised for solids parameterization (sPBEsol), and the other is the charge-only Perdew-Burke-Ernzerhof parameterized generalized gradient approximation with Hubbard U and Hund's J extensions (PBE+U+J) [5–7]. Using both methods, we predict that perovskite $BaMnO_3$ has large Mn off-center displacements and is close to a ferromagnetic-to-antiferromagnetic phase boundary. The reasonable agreement on structural and magnetic properties between sPBEsol and PBE+U+J methods also has important implications in physics. Because PBE+U+J is the mean field limit of PBE+dynamical mean field theory (DMFT); thus the agreement provides additional evidence that building a DMFT theory on a non-magnetic PBE solution is a good way to approach the question of dynamical effects in correlated oxides.

II. COMPUTATIONAL DETAILS

We perform density functional theory calculations [14, 15] within the *ab initio* plane-wave approach [16], as implemented in Vienna Ab-initio Simulation Package (VASP) [17]. We employ projector augmented wave (PAW) pseudopotentials [18, 19]. We use an energy cutoff 600 eV. A $12 \times 12 \times 10$ Monkhorst-Pack grid is used to sample the Brillouin zone of the simulation cell. All the calculations allow for spin-polarization to study different types of long-range magnetic magnetic orderings. Hubbard U corrections are included on Mn $3d$ orbitals [20]. Both cell and internal coordinates are fully relaxed until each force component is smaller than 10 meV/ Å and stress tensor is smaller than 10 kBar.

We study perovskite $Sr_{1-x}Ba_xMnO_3$ using a $\sqrt{2} \times \sqrt{2} \times 2$ simulation cell (shown in Fig. 1) which can accommodate various types of magnetic ordering (see Fig. 10 in the Appendix for details) and allow polar distortions along the [100] and [110] directions. The polar distortion is characterized by the Mn off-center displacement $\vec{\delta}_{\text{Mn-O}}$ which is formally defined as:

$$\vec{\delta}_{\text{Mn-O}} = \frac{1}{6} \sum_{i=1}^{6} \vec{R}_{\text{Mn-O}} \tag{1}$$

where $\vec{R}_{\text{Mn-O}}$ are the vectors connecting a Mn ion to its six nearest oxygen neighbors. In this study, we focus on two specific directions: [100] (Fig. 1**A**, displacement along an Mn-O bond direction) and [110] (Fig. 1**B**, displacement in a MnO_2 plane at 45° to the Mn-O bond direction).

We consider and compare the following exchange correlation functionals: i) local spin density approximation with Hubbard U corrections (LSDA+U) [15]; ii) spin-dependent generalized gradient approximation with Perdew-Burke-Ernzerhof parameterization [21] with Hubbard U corrections (sPBE+U); iii) spin-dependent generalized gradient approximation with Perdew-Burke-Ernzerhof revised for solids parameterization [21] with Hubbard U corrections (sPBEsol+U); iv) charge-only local density approximation with Hubbard U and Hund's J corrections (LDA+U+J); v) charge-only generalized gradient approximation with Perdew-Burke-Ernzerhof parameterization with Hubbard U and Hunds' J corrections (PBE+U+J). In methods i), ii) and iii), the exchange correlation functionals depend on both charge density and spin density. Methods i), ii) and iii) require a double counting correction which depends on both charge and spin densities. Based on previous studies [5–7, 22] which indicate that the spin-dependent exchange correlation functional has a large intrinsic exchange splitting in LSDA, sPBE and sPBEsol, we do not add Hund's J corrections in methods i), ii) and iii). They are implemented in VASP as LDAUTYPE = 2. In methods iv) and v), the exchange correlation functionals only depend on charge density (but not on spin density). Spin symmetry is only broken via the Hubbard U and Hund's J terms. The double counting correction also only depends on charge density. These two methods are implemented in VASP as LDAUTYPE = 4. In method iv) and v), we use $U = 5$ eV and J = 0.7 eV unless otherwise specified.

III.   RESULTS

A.   Perovskite BaMnO_3

Fig. 2 shows the Mn off-center displacements of perovskite BaMnO_3 calculated using the five exchange correlation functionals of interest here. We consider two different magnetic orderings: ferromagnetic ordering, for short F and two sublattice G-type antiferromagnetic ordering, for short G. We find that sPBE and PBE+U+J predict a larger $\delta_{\text{Mn-O}}$ than
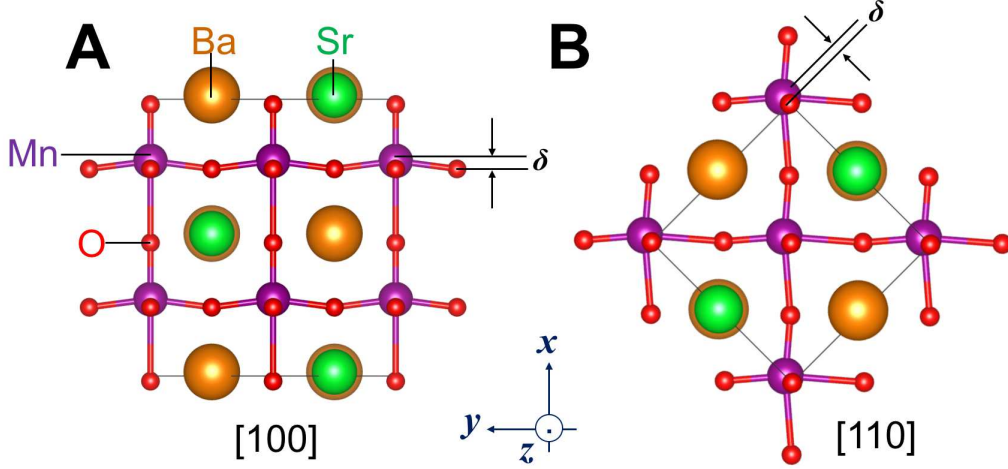
FIG. 1: Atomic structure of perovskite $Sr_{1-x}Ba_xMnO_3$. The orange, green, purple and red balls are Sr, Ba, Mn and O atoms, respectively. **A**) Mn off-center displacement δ along the [100] axis direction. **B**) Mn off-center displacement δ along the [110] axis direction.

LSDA and LDA+U+J, which is consistent with the empirical observation that generalized gradient approximation usually overestimates lattice constants and volumes while local density approximation underestimates lattice constants and volumes. sPBEsol predicts a $\delta_{\text{Mn-O}}$ close to the average value of sPBE and LSDA predictions. The variation of predictions from different exchange correlation functionals is particularly marked for the G-type antiferromagnetic ordering, in which the sPBE and PBE+U+J methods predict $\delta_{\text{Mn-O}}$ to be around 0.2 Å, sPBEsol predicts a $\delta_{\text{Mn-O}}$ to be about 0.1 Å, while LSDA predicts $\delta_{\text{Mn-O}}$ to be around 0.05 Å and LDA+U+J essentially fails to produce a Mn off-center displacement. Our LSDA result is consistent with Ref. [8]. Previous calculations show that typical difference in polar distortions between LDA(LSDA) and PBE(sPBE) is about a factor of 2 [23]. However, for magnetic perovskite $BaMnO_3$, we find that the difference between LSDA and sPBE is much more substantial.

Fig. 3 shows the energy difference between the ferromagnetic and G-type antiferromagnetic states of perovskite $BaMnO_3$ predicted by sPBE+U (squares, blue on-line), sPBEsol+U (triangles, green on-line) and LSDA+U (circles, red on-line) for a wide range of U. We notice that sPBE+U, sPBEsol+U and LSDA+U also make inconsistent predictions for magnetic properties of perovskite $BaMnO_3$. sPBE+U predicts that the ferromagnetic state has lower energy than the G-type antiferromagnetic state for all the values of Hubbard
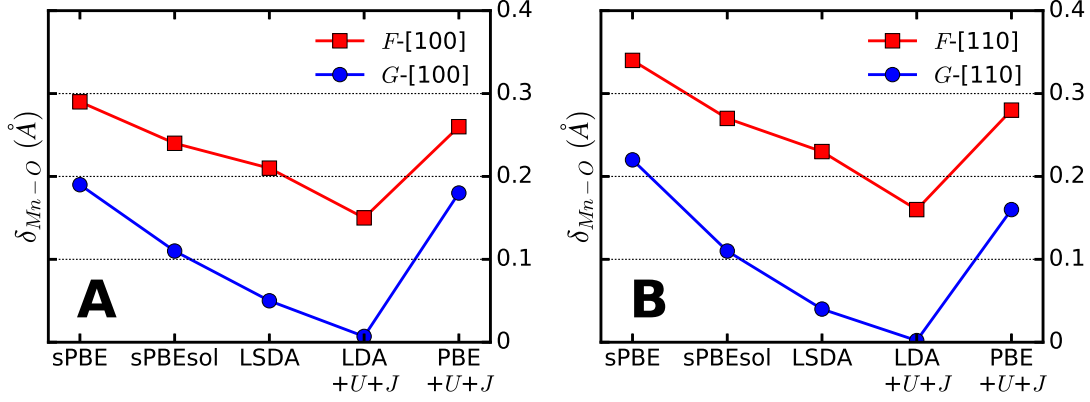
FIG. 2: Mn off-center displacement $\delta_{\text{Mn-O}}$ of perovskite $BaMnO_3$ calculated using different exchange-correlation functionals. sPBE: spin-dependent generalized gradient approximation with Perdew-Burke-Ernzerhof parameterization. sPBEsol: spin-dependent generalized gradient approximation with Perdew-Burke-Ernzerhof revised for solids parameterization. LSDA: local spin density approximation. LDA+U+J: local density approximation with Hubbard U and Hund's J corrections. PBE+U+J: generalized gradient approximation with Perdew-Burke-Ernzerhof parameterization with Hubbard U and Hund's J corrections. $U = 5$ eV and $J = 0.7$ eV. The red curves are for ferromagnetic states and the blue curves are for G-type antiferromagnetic states. **A**) $\delta_{\text{Mn-O}}$ along the [100] direction. **B**) $\delta_{\text{Mn-O}}$ along the [110] direction.

U considered, including $U = 0$, i.e. the ground state from sPBE is predicted to be ferromagnetic, consistent with the previous hypothesis in Ref. [24]. However, LSDA+U predicts that for $0 \leq U \leq 5$ eV, the G-type antiferromagnetic state has lower energy than the ferromagnetic state, consistent with the previous study [8]. In particular, LSDA predicts that the ground state is G-type antiferromagnetic, while sPBE predicts a ferromagnetic state. Just like the structural properties, the prediction of sPBEsol+U (including $U = 0$) sits between sPBE+U and LSDA+U for any given U. The antiferromagnetic-to-ferromagnetic transition point predicted from sPBEsol+U is at $U = 2$ eV. We note that for any given U, the predictions from LSDA+U and sPBE+U on the ferromagnetic-antiferromagnetic energy difference are about 200 meV/Mn apart, which leads to a large uncertainty on prediction for magnetic properties of perovskite $BaMnO_3$.

It is well established in the DFT literature that different functionals predict different unit cell volumes and that unit cell volumes can affect physical properties, in particular

TABLE I: Comparison of fully relaxed structures and relaxed structures with a fixed volume. "xc functional" is the exchange correlation functional. F is the ferromagnetic ordering and G is the G-type antiferromagnetic ordering. $\delta_{\text{Mn-O}}$ is the Mn off-center displacement. $\Delta E = E(G) - E(F)$.

	polar distortions along the [100] direction											
structure	fully relaxed structure						fixed volume					
xc functional	sPBE		sPBEsol		LSDA		sPBE		sPBEsol		LSDA	
magnetic structure	F	G	F	G	F	G	F	G	F	G	F	G
volume Ω (Å^3/ion)	13.21	12.83	12.43	11.92	11.87	11.38	12.54	12.10	12.54	12.10	12.54	12.10
$\delta_{\text{Mn-O}}$ (Å)	0.29	0.19	0.24	0.11	0.21	0.05	0.24	0.12	0.25	0.13	0.26	0.15
ΔE (meV/Mn)	45		-24		-117		51		-23		-92	
	polar distortions along the [110] direction											
structure	fully relaxed structure						fixed volume					
xc functional	sPBE		sPBEsol		LSDA		sPBE		sPBEsol		LSDA	
magnetic structure	F	G	F	G	F	G	F	G	F	G	F	G
volume Ω (Å^3/ion)	13.37	12.86	12.46	11.92	11.86	11.37	12.61	12.11	12.61	12.11	12.61	12.11
$\delta_{\text{Mn-O}}$ (Å)	0.34	0.22	0.27	0.11	0.23	0.04	0.28	0.13	0.29	0.15	0.30	0.15
ΔE (meV/Mn)	62		-22		-120		65		-16		-98	

ferroelectric polarization [3, 4, 23]. However, volume effects alone do not explain the difference in predictions of magnetic properties. We present in Table I both calculations for fully relaxed structures and calculations at a fixed unit cell volume (chosen as the average of relaxed sPBE and LSDA volumes). As Table I shows, for the fully relaxed structures, sPBE predicts the largest unit cell volume, LSDA predicts the smallest unit cell volume and sPBEsol predicts a unit cell volume which is close to the average value of sPBE and LSDA predictions. The larger volume leads to a larger $\delta_{\text{Mn-O}}$, and the larger $\delta_{\text{Mn-O}}$ favors ferromagnetism [12, 25]. This trend is evidently shown in the energy difference ΔE between the ferromagnetic ordering and the G-type antiferromagnetic ordering. At a fixed unit cell volume for each magnetic ordering, the $\delta_{\text{Mn-O}}$ predicted by the three methods become almost identical, but sPBE and LSDA still make opposite predictions for the energy stability
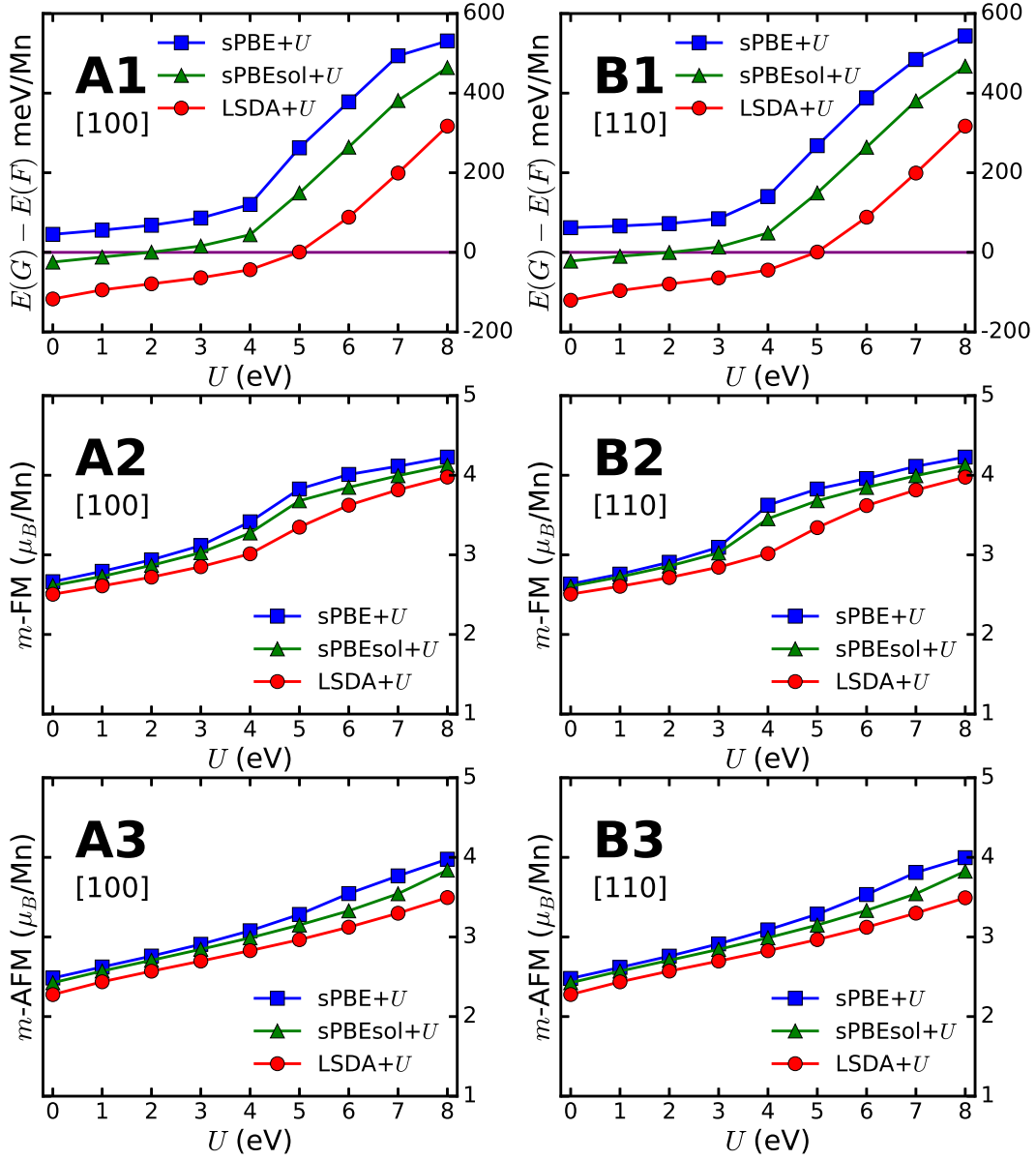
FIG. 3: Energy difference of perovskite $BaMnO_3$ between the ferromagnetic state and G-type antiferromagnetic state $E(F) - E(G)$ with Mn off-center displacement along the [100] direction (panel **A**) and Mn off-center displacement along the [110] direction (panel **B**), calculated using sPBE+U (blue curves with square symbols), sPBEsol+U (green curves with triangle symbols) and LSDA+U (red curves with circle symbols).
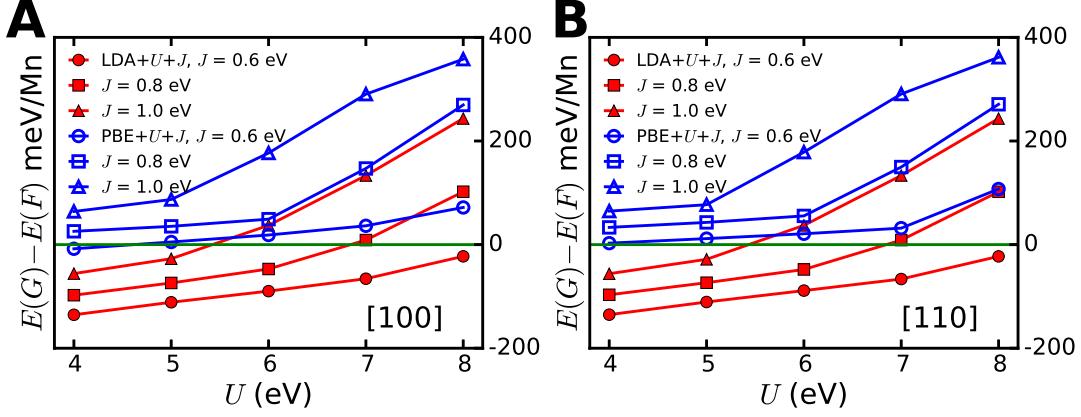
FIG. 4: Energy difference of perovskite $BaMnO_3$ between the ferromagnetic state and G-type antiferromagnetic state $E(F) - E(G)$ calculated using PBE+U+J (blue curves with symbols) and LDA+U+J (red curves with symbols). **A**) Mn off-center displacement along the [100] direction. **B**) Mn off-center displacement along the [110] direction.

between ferromagnetic and G-type antiferromagnetic states.

Fig. 4 compares the predictions of LDA+U+J (red curves) and PBE+U+J (blue curves) for the energy difference between ferromagnetic ordering and G-type antiferromagnetic ordering for perovskite $BaMnO_3$ for a range of U and J. Increasing U and J generically favors the ferromagnetism [26]. We see that the results are very similar to those shown in Fig. 3. PBE+U+J favors the ferromagnetic state substantially more than LDA+U+J does.

B.   Perovskite $Sr_{0.5}Ba_{0.5}MnO_3$

Perovskite $BaMnO_3$ has not been successfully synthesized in experiment because the ground state structure of $BaMnO_3$ is a hexagonal polymorph [11, 27]. However, perovskite $Sr_{0.5}Ba_{0.5}MnO_3$ alloy has been experimentally stabilized [13]. At low temperatures, the material is experimentally found to be a G-type antiferromagnet with a ferroelectric polarization which originates from Mn off-center displacements δ_{Mn-O} (defined in Eq. (1)) along the [100] direction [13]. This material therefore provides a way to benchmark different exchange correlation functionals. Fig. 5 presents the magnetic energy difference between the ferromagnetic ordering and the G-type antiferromagnetic ordering of $Sr_{0.5}Ba_{0.5}MnO_3$ for δ_{Mn-O} along the [100] and [110] directions. Since experimentally the polarization is along the [100] direction, we focus on Fig. 5**A**. Consistent with the previous discussion on Fig. 3 and
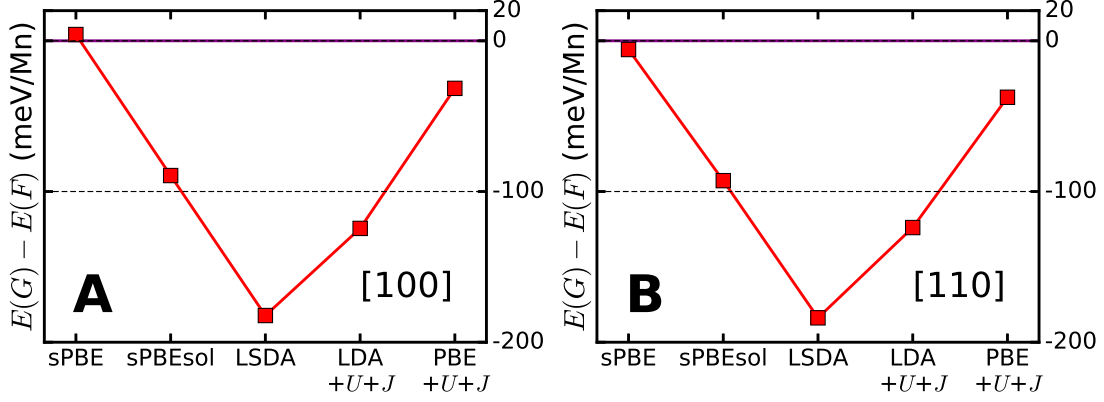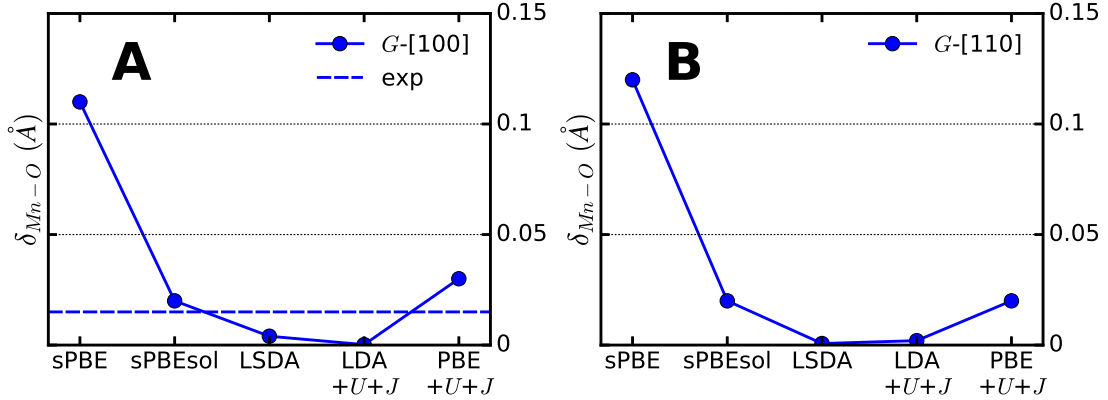
9

FIG. 5: Energy difference of perovskite $Sr_{0.5}Ba_{0.5}MnO_3$ between the ferromagnetic state (F) and G-type antiferromagnetic state (G) calculated using different exchange-correlation functionals. sPBE, sPBEsol, LSDA, LDA+U+J and PBE+U+J have the same meaning as those in Fig. 2. $U = 5$ eV and $J = 0.7$ eV are used in LDA+U+J and PBE+U+J methods. **A**) Mn off-center displacement along the [100] direction. **B**) Mn off-center displacement along the [110] direction.

FIG. 6: Mn off-center displacement $\delta_{\text{Mn-O}}$ of perovskite $Sr_{0.5}Ba_{0.5}MnO_3$ calculated using different exchange-correlation functionals. The notations of sPBE, sPBEsol, LSDA, LDA+U+J and PBE+U+J have the same meaning as those in the caption of Fig. 2. $U = 5$ eV and $J = 0.7$ eV are used in LDA+U+J and PBE+U+J methods. The blue dashed line is the experimental value of $\delta_{\text{Mn-O}}$ of the G-type antiferromagnetic state with the polarization along the [100] direction.

Fig. 4, PBE-type exchange correlation functionals favor ferromagnetism more than LDA-type exchange correlation functionals. However, sPBE predicts that for $Sr_{0.5}Ba_{0.5}MnO_3$ with the $\delta_{\text{Mn-O}}$ along the [100] direction, the ferromagnetic state has slightly lower energy than
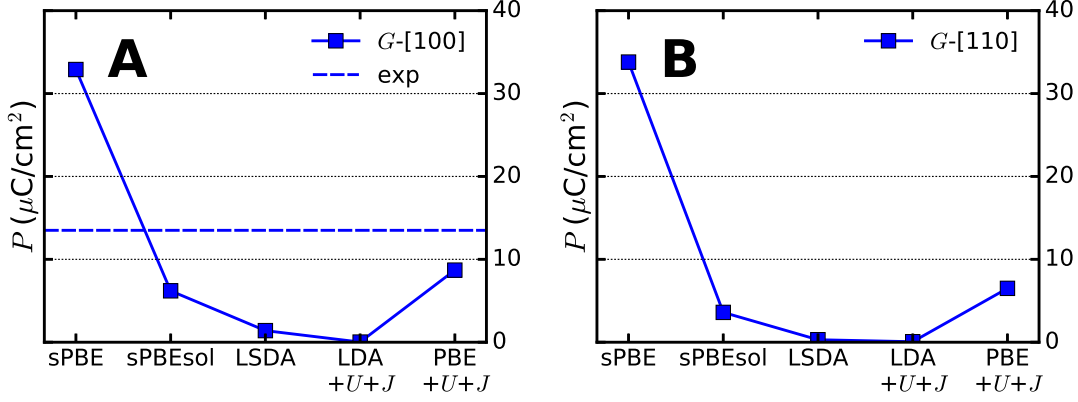
FIG. 7: Polarization P of perovskite $Sr_{0.5}Ba_{0.5}MnO_3$ calculated using different exchange-correlation functionals. The notations of sPBE, sPBEsol, LSDA, LDA+U+J and PBE+U+J as well as the symbols have the same meaning as those in the caption of Fig. 2. $U = 5$ eV and $J = 0.7$ eV are used in LDA+U+J and PBE+U+J methods. The blue dashed line is the experimental values of P of the G-type antiferromagnetic state with the polarization along the [100] direction.

the G-type antiferromagnetic state, which is inconsistent with the experiment. The other four exchange correlation functionals predict that the G-type antiferromagnetic state is the ground state of $Sr_{0.5}Ba_{0.5}MnO_3$.

Fig. 6 presents the Mn off-center displacement δ_{Mn-O}, calculated using the five exchange correlation functionals considered in this study. The measured low temperature Mn off-center displacement of 0.015 Å along the [100] direction is shown as the dashed blue line in panel **A** [13]. We see that sPBE predicts the δ_{Mn-O} to be 0.11 Å, almost one order of magnitude larger than the experiment. On the other hand, LSDA and LDA+U+J essentially fail to produce a Mn off-center displacement, predicting tiny values of 4×10^{-3} Å and 2×10^{-4} Å, respectively. PBE+U+J predicts the δ_{Mn-O} to be 0.03 Å, a factor of 2 larger than the experiment and sPBEsol predicts a δ_{Mn-O} of 0.02 Å, which is closest to the experimental value.

Fig. 7 presents the polarization of the G-type antiferromagnetic state of $Sr_{0.5}Ba_{0.5}MnO_3$. The experimental value of the [100] polarization in the observed G-type antiferromagnetic state is 13.5 $\mu C/cm^2$ [13]. LSDA, sPBEsol, sPBE, LDA+U+J and PBE+U+J predict a polarization of 1.4 $\mu C/cm^2$, 6.2 $\mu C/cm^2$, 32.9 $\mu C/cm^2$, 0.02 $\mu C/cm^2$ and 8.7 $\mu C/cm^2$, respectively. By comparison, PBE+U+J and sPBEsol produce the best and second best

agreement with the experiment. Based on this comparison between theory and experiment, we suggest that both PBE+U+J and sPBEsol are the two exchange correlation functionals that best describes both magnetic and structural properties of $Sr_{0.5}Ba_{0.5}MnO_3$, which implies that they may also reasonably describe $Sr_{1-x}Ba_xMnO_3$ with other values of x. Using both PBE+U+J and sPBEsol, we find that the ground state of perovskite $BaMnO_3$ has large Mn off-center displacements [25] and it is much closer to the ferromagnetic-to-antiferromagnetic phase boundary than was predicted by previous LSDA calculations [8].

IV. DISCUSSION

In this section, we discuss the magnetic phase diagram spanned by Hubbard U and Hund's J calculated with the PBE+U+J method. We restrict our attention to 0.55 eV $\leq J \leq$ 1.05 eV and to 4 eV $\leq U \leq$ 8.5 eV. Both ranges are consistent with constrained random-phase-approximation (c-RPA) calculations on the related materials [28, 29]. For U smaller than 4 eV (not shown), the calculations fail to produce a fully spin-polarized Mn d states [7], which is inconsistent with experiments. Results are shown in Fig. 8. A first important result is that for $U + 5J \lesssim 10$ eV, we consistently find a noncentrosymmetric state characterized by a non-zero $\delta_{Mn\text{-}O}$ while for $U + 5J \gtrsim 10$ eV, the predicted phase is ferromagnetic, metallic and centrosymmetric. We believe that the regime $U + 5J \gtrsim 10$ eV is not physically relevant since calculations with U and J in this range fail to reproduce the Mn off-center displacements that are experimentally observed in $Sr_{0.5}Ba_{0.5}MnO_3$ [13] (see Fig. 11 in the Appendix). Thus we believe that the prediction that perovskite $BaMnO_3$ has a non-centrosymmetric ground state is robust against variation of U and J in the physically reasonable range, which is consistent with the previous studies on perovskite manganite oxides [8–10, 13].

A second point is that within the PBE+U+J methodology the ferromagnetic non-centrosymmetric phase may be metallic if $\delta_{Mn\text{-}O}$ is along the [100] direction or insulating with a band gap of about 0.5 eV if $\delta_{Mn\text{-}O}$ is along the [110] direction. Fig. 9 compares the density of states between the $\delta_{Mn\text{-}O}$ along the [100] direction and that along the [110] direction. The results in Fig. 9 are calculated using $U = 5$ eV and $J = 0.7$ eV. We also test other values of U and J (see Fig. 12 in the Appendix), which do not significantly change the density of states. A metallic noncentrosymmetric state has been theoretically predicted and
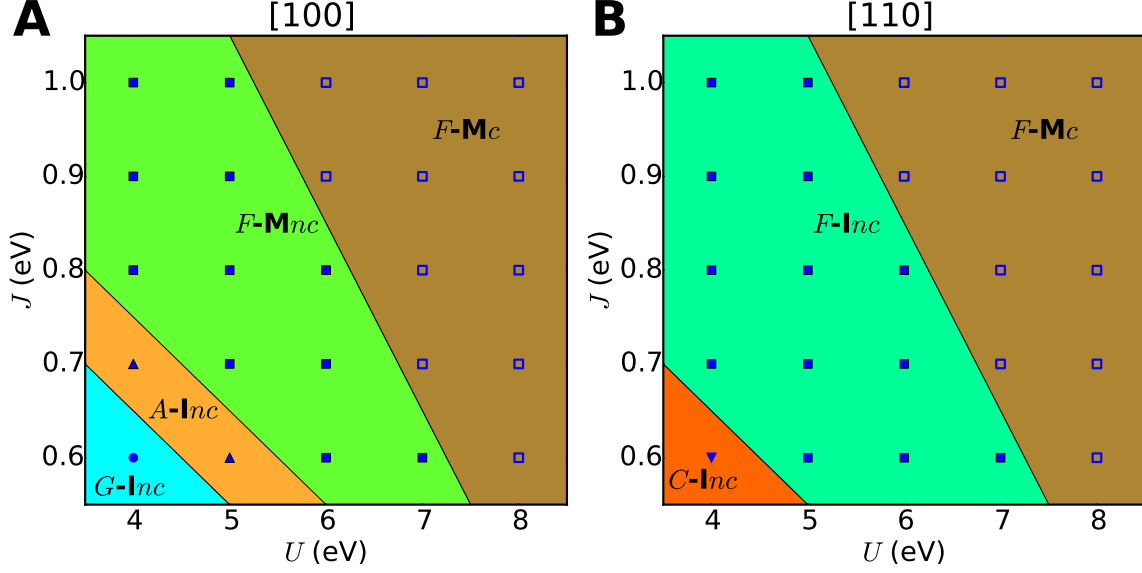
FIG. 8: Phase diagram showing properties of minimum energy state of perovskite $BaMnO_3$ predicted by PBE+U+J calculations for Mn off-center displacements along the **A**) [100] and **B**) [110] directions, computed in the Hubbard-U and Hund's-J plane. Points at which computations are performed are indicated by small geometric shapes. Different phases (phase boundaries inferred) are indicated by symbol shapes, labels and colors. The light blue patch with circle symbols denotes G-type anti-ferromagnetic insulating noncentrosymmetric state (G-**I**nc); the orange patch with up-triangle symbols denotes A-type anti-ferromagnetic insulating noncentrosymmetric state (A-**I**nc); the red patch with down-triangle symbols denotes C-type anti-ferromagnetic insulating noncentrosymmetric state (C-**I**nc); the light green patch with solid square symbols denotes ferromagnetic metallic noncentrosymmetric state (F-**M**nc); the dark green patch with solid square symbols denotes ferromagnetic insulating noncentrosymmetric state (F-**I**nc); the brown patch with open square symbols denotes ferromagnetic metallic centrosymmetric state (F-**M**c). See Fig. S5 and Fig. S6 in the Supplementary Materials for details.

experimentally observed in other materials [30–34] and if it occurred only for one direction of Mn off-center displacement in this system, the consequences would be very interesting because a metal-insulator transition could be driven by rotating the direction of polarizations. However, we need to comment that as seen in Fig. 9, the metallicity occurs because the highest occupied O p bands and lowest unoccupied Mn d bands just barely overlap, so the density of states at the Fermi level is small. Since DFT-PBE usually underestimates band
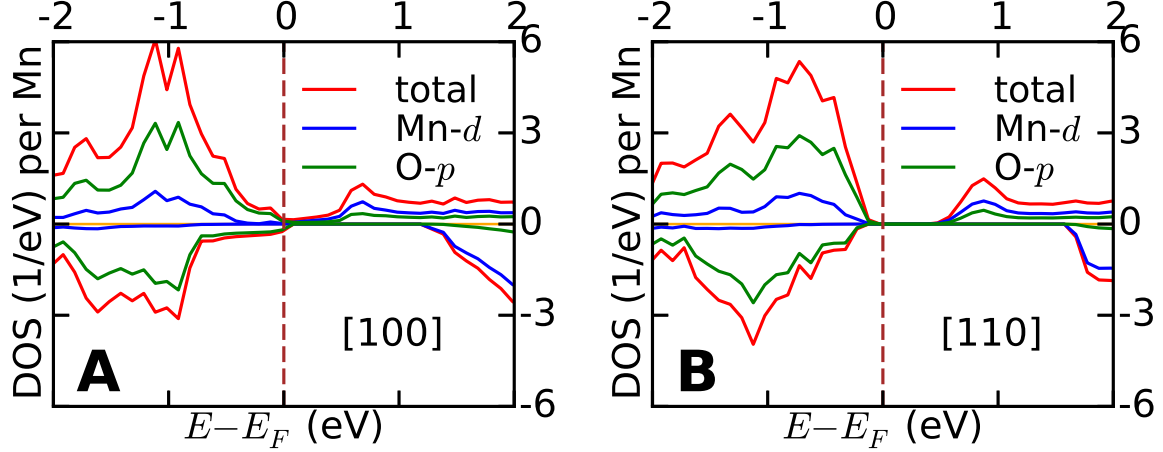
FIG. 9: Density of states of perovskite $BaMnO_3$, calculated using PBE+U+J with $U = 5$ eV and $J = 0.7$ eV. The red, blue and green curves are total density of states, Mn-d projected density of states and O-p projected density of states. **A**) Mn off-center displacement along the [100] direction. **B**) Mn off-center displacement along the [110] direction.

gaps, the metallic noncentrosymmetric state found for $\delta_{\text{Mn-O}}$ along the [100] direction might be an artifact. However the prediction of a difference in transport properties between the [100] and [110] directions, with the [110] state being more insulating, is likely to be robust, implying significant variations in resistivity with different polarization directions. Further investigation of this issue is an interesting challenge for future research.

Generically we see that as U and J are increased, there is an antiferromagnet-to-ferromagnetic transition. The transition occurs because increasing U and J increases the energy denominator relevant to Mn t_{2g}-to-t_{2g} superexchange and thus suppresses antiferromagnetism. Ferromagnetism is driven by double exchange involving the e_g orbitals; this is favored by increasing J and is less affected by U because it involves the e_g orbitals which have a larger admixture of oxygen. As U increases, there is also a tendency for the amplitude of polar distortions to decrease. The decrease occurs because larger U reduces the hybridization between Mn d and O p states, which disfavors the off-centering of Mn atom [8–10, 13].

Finally, we comment that sPBEsol predicts that the ground state of perovskite $BaMnO_3$ is antiferromagnetic, while adding a Hubbard U extension leads a ferromagnetic state as $U \geq 2$ eV. The PBE+U+J method predicts both ferromagnetic and antiferromagnetic states depending on the Hubbard U and Hund's J. Based on both methods, we predict perovskite $BaMnO_3$ is close to the antiferromagnetic-to-ferromagnetic phase boundary. There-

14

fore, when under epitaxial strain, perovskite $BaMnO_3$ is a promising candidate to observe the long-sought giant effective magnetoelectric effects and cross-field control of polarization and magnetism [12].

V. CONCLUSION

In conclusion, our systematic study of the predictions of different exchange correlation functionals for structural and magnetic properties of a representative class of magnetic ferroelectrics reveals that the widely used exchange correlation functionals LSDA and sPBE predict different structural and magnetic properties for perovskite $BaMnO_3$ and $Sr_{0.5}Ba_{0.5}MnO_3$. By comparing with the available experimental data of $Sr_{0.5}Ba_{0.5}MnO_3$, we establish that adding Hubbard U and Hund's J corrections to the charge-only Perdew-Burke-Ernzerhof parameterized generalized gradient approximation (PBE+U+J) and spin-dependent generalized gradient approximation with Perdew-Burke-Ernzerhof revised for solids parameterization (sPBEsol) both improve the predictions over LSDA and sPBE and yield the best theory-experiment agreement. Using both methods, we find that perovskite $BaMnO_3$ has large Mn off-center displacements and is close to an antiferromagnetic-to-ferromagnetic phase boundary, which makes perovskite $BaMnO_3$ and related-compounds promising candidates to induce the long-sought giant effective magnetoelectric effects [12].

Experimentally, perovskite $Sr_{1-x}Ba_xMnO_3$ with $x > 0.5$ has not been synthesized. We hope that the theoretically predicted multiferroic properties of perovskite $BaMnO_3$ could stimulate further experiments. If the material can be stabilized in experiment, the comparison of the measured structures and magnetism with the calculated ones can shed light on the approximations of exchange correlation functionals in density functional theory computations.

Computing Center.

Appendix A: Magnetic ordering

In this study, we consider four types of magnetic orderings: ferromagnetic ordering (F), A-type anti-ferromagnetic ordering, C-type anti-ferromagnetic ordering and G-type anti-ferromagnetic ordering. The arrangement of spins for each magnetic ordering is shown in Fig. 10.
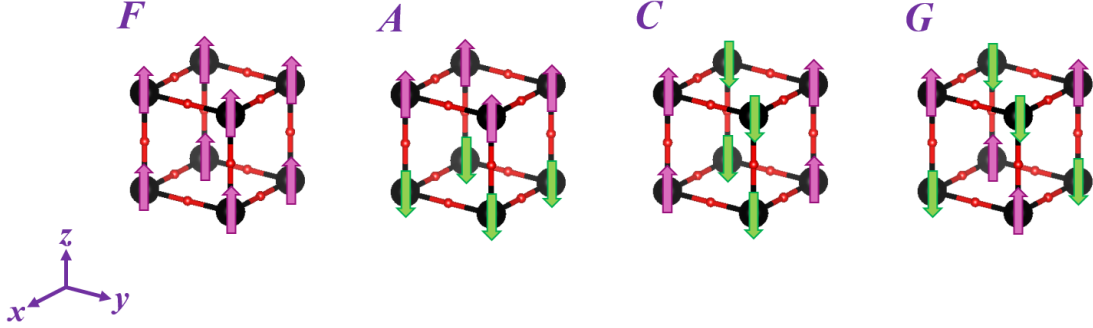

FIG. 10: Arrangment of spins for different magnetic orderings. **A**) ferromagnetic ordering. **B**) A-type anti-ferromagnetic ordering. **C**) C-type anti-ferromagnetic ordering. **D**) G-type anti-ferromagnetic ordering.

Appendix B: Mn off-center displacements in $Sr_{0.5}Ba_{0.5}MnO_3$ using PBE+U+J

Fig. 11 shows the Mn off-center displacement in $Sr_{0.5}Ba_{0.5}MnO_3$ calculated using PBE+U+J method. In the phase diagram spanned by (U, J), there is a boundary that separates a centrosymmetric phase and a non-centrosymmetric phase.
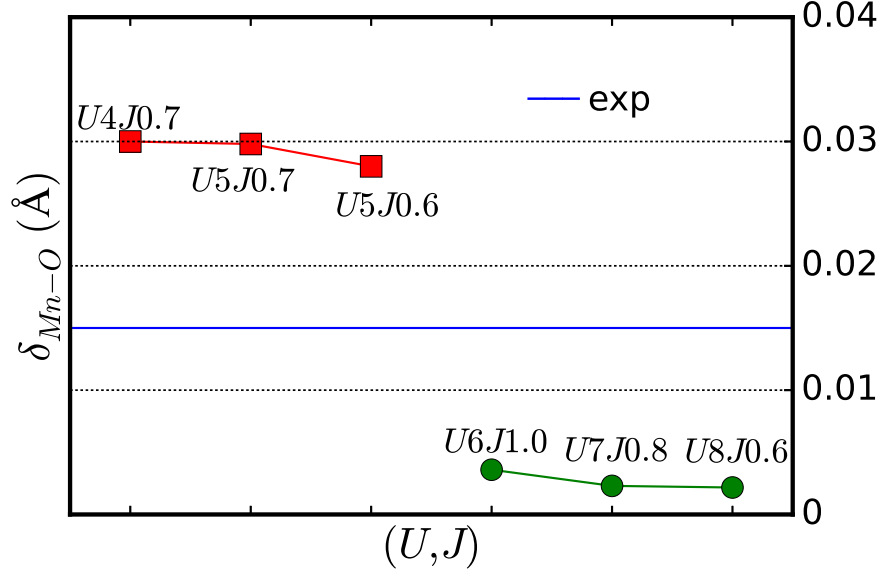

FIG. 11: Mn off-center displacement $\delta_{Mn\text{-}O}$ calculated using PBE+U+J. The red symbols are those (U, J) values that yield a Mn off-center displacement in $Sr_{0.5}Ba_{0.5}MnO_3$. The green symbols are those (U, J) values that fail to reproduce the Mn off-center displacement in $Sr_{0.5}Ba_{0.5}MnO_3$. The unit of U and J is eV. The blue solid line is the experimental results from Ref. [13].

Appendix C: Density of state of BaMnO$_3$ using PBE+U+J

Fig. 12 shows the representative density of states of BaMnO$_3$ for ferromagnetic-noncentrosymmetric states using different U and J values. The robust feature is that the state with the Mn off-center displacement $\delta_{\text{Mn-O}}$ along the [100] direction has a vanishing band gap, while the state with $\delta_{\text{Mn-O}}$ along the [110] direction has a band gap of about 0.5 eV.
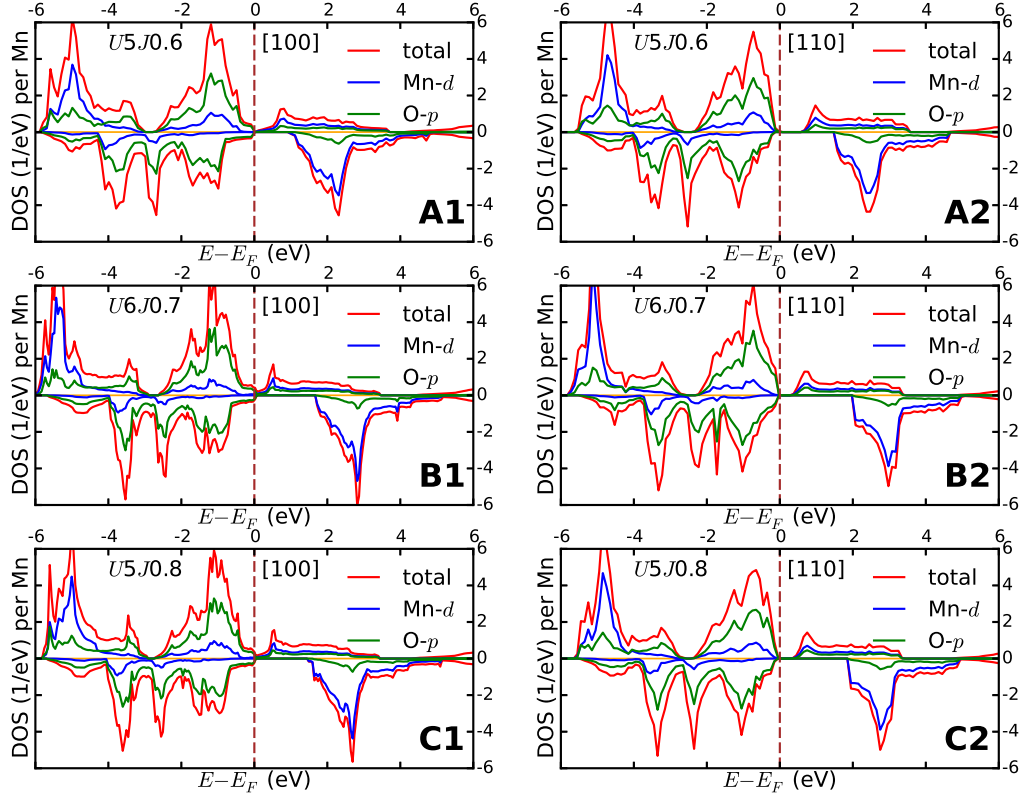
FIG. 12: Density of states of ferromagnetic-noncentrosymmetric perovskite BaMnO$_3$. The red, blue and green curves are total, Mn d projected and O p projected density of states, respectively. The brown dashed line is the Fermi level. Panels **A**: using $U = 5$ eV and $J = 0.6$ eV. **A1**) Mn off-center displacement along the [100] direction. **A2**) Mn off-center displacement along the [110] direction. Panels **B**: using $U = 6$ eV and $J = 0.7$ eV. **B1**) Mn off-center displacement along the [100] direction. **B2**) Mn off-center displacement along the [110] direction. Panels **C**: using $U = 5$ eV and $J = 0.8$ eV. **C1**) Mn off-center displacement along the [100] direction. **C2**) Mn off-center displacement along the [110] direction.

[1] W. Eerenstein, N. D. Mathur, and J. F. Scott, Nature **442**, 759 (2006).

[2] R. Ramesh and N. A. Spaldin, Nat. Mater. **6**, 21 (2007).

[3] Z. Wu, R. E. Cohen, and D. J. Singh, Phys. Rev. B **70**, 104112 (2004).

[4] Z. Wu and R. E. Cohen, Phys. Rev. B **73**, 235116 (2006).

[5] H. Park, A. J. Millis, and C. A. Marianetti, Phys. Rev. B **92**, 035146 (2015).

[6] J. Chen, A. J. Millis, and C. A. Marianetti, Phys. Rev. B **91**, 241111 (2015).

[7] H. Chen and A. J. Millis, Phys. Rev. B **93**, 045133 (2016).

[8] J. M. Rondinelli, A. S. Eidelson, and N. A. Spaldin, Phys. Rev. B **79**, 205119 (2009).

[9] G. Giovannetti, S. Kumar, C. Ortix, M. Capone, and J. van den Brink, Phys. Rev. Lett. **109**, 107601 (2012).

[10] R. Nourafkan, G. Kotliar, and A.-M. S. Tremblay, Phys. Rev. B **90**, 220405 (2014).

[11] R. Søndenå, S. Stølen, P. Ravindran, T. Grande, and N. L. Allan, Phys. Rev. B **75**, 184105 (2007).

[12] J. H. Lee and K. M. Rabe, Phys. Rev. Lett. **104**, 207204 (2010).

[13] H. Sakai, J. Fujioka, T. Fukuda, D. Okuyama, D. Hashizume, F. Kagawa, H. Nakao, Y. Murakami, T. Arima, A. Q. R. Baron, et al., Phys. Rev. Lett. **107**, 137601 (2011).

[14] P. Hohenberg and W. Kohn, Phys. Rev. **136**, B864 (1964).

[15] W. Kohn and L. J. Sham, Phys. Rev. **140**, A1133 (1965).

[16] M. C. Payne, M. P. Teter, D. C. Allan, T. A. Arias, and J. D. Joannopoulos, Rev. Mod. Phys. **64**, 1045 (1992).

[17] G. Kresse and J. Furthmüller, Phys. Rev. B **54**, 11169 (1996).

[18] P. E. Blöchl, Phys. Rev. B **50**, 17953 (1994).

[19] G. Kresse and D. Joubert, Phys. Rev. B **59**, 1758 (1999).

[20] A. I. Liechtenstein, V. I. Anisimov, and J. Zaanen, Phys. Rev. B **52**, R5467 (1995).

[21] J. P. Perdew, K. Burke, and M. Ernzerhof, Phys. Rev. Lett. **77**, 3865 (1996).

[22] H. Chen and A. J. Millis, unpublished results.

[23] D. I. Bilc, R. Orlando, R. Shaltaf, G.-M. Rignanese, J. Íñiguez, and P. Ghosez, Phys. Rev. B **77**, 165107 (2008).

[24] J. Hong, A. Stroppa, J. Íñiguez, S. Picozzi, and D. Vanderbilt, Phys. Rev. B **85**, 054417

(2012).

[25] H. Chen and A. Millis, arXiv:1509.06650 (2015).

[26] H. Chen and A. Millis, arXiv:1511.06042 (2015).

[27] R. Søndenå, P. Ravindran, S. Stølen, T. Grande, and M. Hanfland, Phys. Rev. B **74**, 144102 (2006).

[28] L. Vaugier, H. Jiang, and S. Biermann, Phys. Rev. B **86**, 165105 (2012).

[29] F. Aryasetiawan, M. Imada, A. Georges, G. Kotliar, S. Biermann, and A. I. Lichtenstein, Phys. Rev. B **70**, 195104 (2004).

[30] P. W. Anderson and E. I. Blount, Phys. Rev. Lett. **14**, 217 (1965).

[31] D. Puggioni and J. M. Rondinelli, Nat. Commun. **5**, 3432 (2014).

[32] Y. Wang, X. Liu, J. D. Burton, S. S. Jaswal, and E. Y. Tsymbal, Phys. Rev. Lett. **109**, 247601 (2012).

[33] T. Kolodiazhnyi, M. Tachibana, H. Kawaji, J. Hwang, and E. Takayama-Muromachi, Phys. Rev. Lett. **104**, 147602 (2010).

[34] Y. Shi, Y. Guo, X. Wang, A. J. Princep, D. Khalyavin, P. Manuel, Y. Michiue, A. Sato, K. Tsuda, S. Yu, et al., Nat. Mater. **12**, 1024 (2013).